Doping dependence of thermoelectric performance in Mo_3Sb_7: First-principles calculations

David Parker, Mao-Hua Du, and David J. Singh
Oak Ridge National Laboratory, 1 Bethel Valley Road, Oak Ridge, Tennessee 37831, USA
(Received 28 December 2010; revised manuscript received 22 February 2011; published 20 June 2011)

We study the effects of doping Mo_3Sb_7 with transition metals (Ni, Fe, Co, Ru) via first-principles calculations, including electronic structure, lattice dynamics, and Boltzmann transport. We find heavy-mass bands and large, rapidly varying density of states, generally favorable for high thermopower, near the band gap of this material. Transport calculations predict large Seebeck coefficients exceeding 300 μV/K in a wide temperature range above 500 K (a range suitable for waste heat recovery), if the material can be doped into a semiconducting state. These thermopowers are much higher than those that have previously been experimentally observed; we find that performance exceeding current limits may be found at lower carrier concentration than achieved presently. We also discuss the selection of dopant and the potential thermoelectric performance of optimally doped Mo_3Sb_7.

DOI: 10.1103/PhysRevB.83.245111 PACS number(s): 72.20.Pa

I. INTRODUCTION

The many conflicting requirements for a good thermoelectric material[1] make the search for usable, practical materials—those with the dimensionless figure-of-merit ZT substantially exceeding unity—a great challenge spanning five decades of research. Mo_3Sb_7 is an interesting material from this point of view, with a ZT of 0.93 already found[2] for a nickel- and tellurium- doped Mo_3Sb_7. Experimental and theoretical work (i.e., band-structure calculations) indicates that the undoped material has metallic character, with several bands crossing the Fermi level, but with a band gap at an electron count somewhat above that of the pure compound. Of great interest, the high ZT value found was at a carrier hole concentration of 5×10^{21} cm^{-3}, much higher than where optimal thermoelectric performance is usually found. This suggests that Mo_3Sb_7 could exhibit even better thermoelectric performance if carrier concentration were reduced by further doping into a semiconducting state. In this paper, we will describe first-principles calculations of electronic structure and Boltzmann transport, supplemented with lattice-dynamics calculations, of the Mo_3Sb_7 material, alloyed toward a semiconducting state with a number of transition metals. We find, based on the analysis presented in the following sections, that excellent thermoelectric performance can be attained if lower carrier concentrations can be achieved.

Several efforts have been devoted toward doping this material, both on the Mo site and on the Sb site, in an attempt to improve the thermoelectric properties, which are generally not optimal for an undoped metallic compound such as Mo_3Sb_7. For this compound, 800 K thermopower[3] does not exceed 60 μV/K. Iron, nickel, ruthenium, manganese, and cobalt have all been doped on the Mo site,[4–7] while several efforts have alloyed the Sb site with its Periodic Table neighbor Te,[8–10] and some work has been done with alloying on both sites.[2,11] Only p-type material has been synthesized. Thermopowers as high as 200 μV/K (Ref. 9) have been observed at high temperature, and substantial ZT's—exceeding 0.5—have been found in more than one experiment. As mentioned above, in Ref. 2 a figure-of-merit ZT (see Ref. 12 for the definition of this quantity) of 0.93 at 1023 K was found for $Ni_{0.06}Mo_3Sb_{5.4}Te_{1.6}$, at a very high hole carrier concentration (roughly 5×10^{21} cm^{-3}). The corresponding maximum ZT for doping on the Mo site is 0.55, and was achieved at a significantly greater carrier concentration of 7×10^{21} cm^{-3}. As is the case with these data, the Seebeck coefficient—a key parameter for any thermoelectric—generally increases as carrier concentration is reduced. Such a reduction in carrier concentration would also tend to cause the maximum ZT to occur at lower temperatures, which is of importance because ZT is still rising rapidly at the highest temperatures in the Te-doped and Mo-site doped materials. These facts together mean it is highly likely that better performance for higher Mo-site doping (leading to lower hole concentrations) can be achieved. This is particularly true in view of possible solubility limits of individual dopants, which may indicate the use of codoping.

Despite the relative success of the work completed to date, it is clear that the Mo_3Sb_7 materials are far from optimized, and there is a notable dearth of information about what constitutes "optimal" doping, about the performance attainable at this doping, and the effect of different dopants on this optimal performance. In this work, we provide information about the likely effects of doping on the thermoelectric properties.

We have three main findings:

(i) High-temperature thermopowers above 300 μV/K are attainable in a wide range of hole concentration.
(ii) The doping range for optimal performance is approximately $p = (9 \times 10^{19})$–(4.6×10^{20}) cm^{-3}.
(iii) All the dopants studied—Co, Fe, Ni, and Ru—are likely to be useful for doping the material.

The highest ZT value to date has been obtained on a sample doped with tellurium to replace the antimony. However, a practical concern with Te arises: it is a trace element, with limited availability.[13] This makes it highly unlikely that a Te-doped material could be used in large-scale applications such as automotive waste heat recovery or thermoelectric solar cells. For this reason, we choose to focus here on doping of the Mo site with comparatively cheap, commonly available transition metals such as iron, nickel, and cobalt. For completeness, we also include the substantially more expensive ruthenium.

 ©2011 American Physical Society

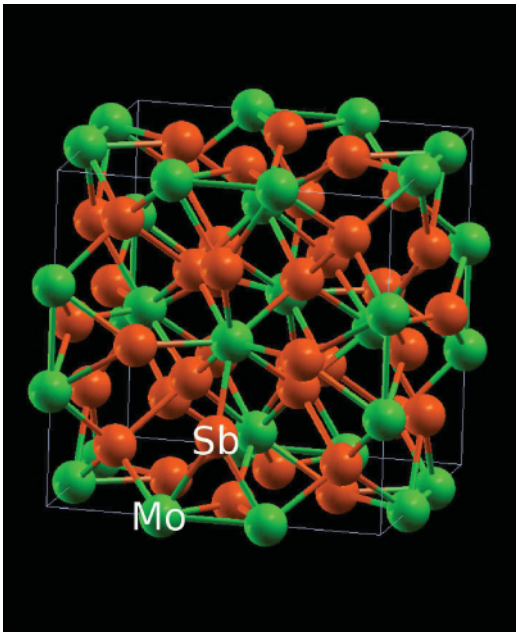

FIG. 1. (Color online) A plot of the chemical structure of Mo_3Sb_7.

II. MODEL AND CALCULATED ELECTRONIC STRUCTURE AND TRANSPORT RESULTS

Our calculations are based on the generalized gradient approximation (GGA) of density functional theory as implemented in WIEN2K,[14] along with a Boltzmann transport code, "BOLTZTRAP,"[15] for calculating the thermopower, and the FROPHO frozen phonon code[16] for lattice dynamics. We have run to self-consistency calculations for the parent compound Mo_3Sb_7, both in the actual configuration of this material and within the virtual crystal approximation (VCA),[17] where the the addition of dopants is modeled by adding an additional charge of $2/3e^-$ per Mo atom, resulting in a filling of the band. We depict the chemical structure of Mo_3Sb_7 in Fig. 1.[18] In addition, we have run calculations of the band structure, density of states, and lattice dynamics of the hypothetical compounds "$Mo_{2.5}A_{0.5}Sb_7$," with A = cobalt, nickel, iron, or ruthenium, with the actual atomic charge used for these calculations; we have also performed calculations for "Mo_2FeSb_7." All calculations, with the exception of the phonon calculations, include spin-orbit coupling as well as force optimization (to forces less than 2 milli-Rydberg/Bohr radius) of the internal coordinates, with the force optimization performed using the pseudopotential code VASP. The lattice parameter has been set throughout to the experimental value for Mo_3Sb_7.

All self-consistency calculations were performed with between 200 and 2000 k points in the full Brillouin zone, while the transport calculations were performed with approximately 20 000 k points in the full Brillouin zone. The Seebeck coefficient, isotropic due to the cubic symmetry, was calculated for Mo_3Sb_7 within the VCA, as described above, as well as for a "rigid band" shift, in which the band structure is assumed not to change with doping, with only E_F changing. We have used throughout the constant relaxation-time approximation, within which the electron scattering time is assumed independent of energy. This approximation allows for quantitatively

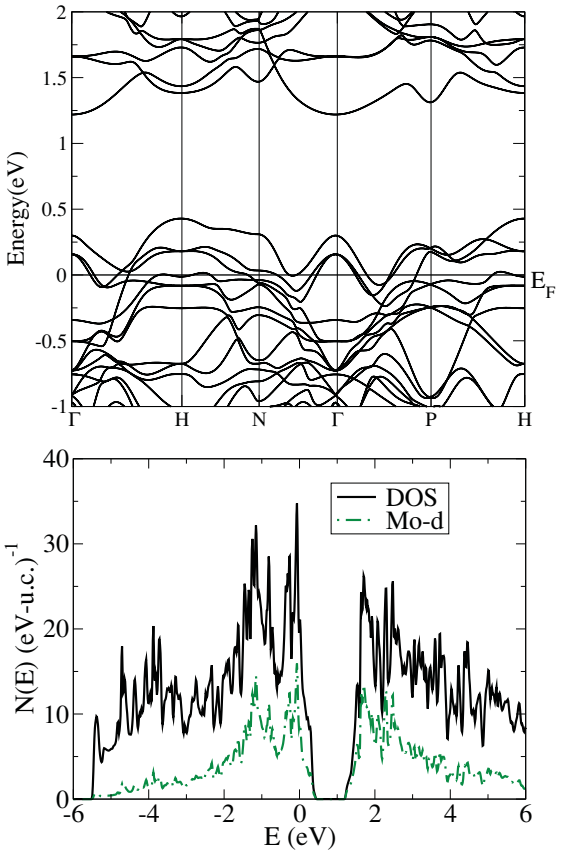

FIG. 2. (Color online) (Top) The calculated first-principles band structure for Mo_3Sb_7. (Bottom) The density of states for this compound, with the Mo d-character weighting shown as well.

accurate[19,20] calculations of the Seebeck coefficient S without additional assumptions about the scattering; as described in Ref. 21, the scattering time drops out of the calculation of S so we need not even know its magnitude.

In Fig. 2(a), we present our calculated results for the band structure of this compound, which shows a gap of roughly 0.8 eV beginning approximately 0.4 eV above the Fermi level, in accordance with other published results for the band structure of this compound. In Fig. 2(b), we have plotted the density of states (DOS) in the vicinity of the Fermi level and the gap. There is a comparatively high DOS very near to the band gap. This derives from the generally heavy bands near the band edge; in Fig. 2(a) one sees overall dispersions of the valence and conduction bands nearest the gap of less than 0.5 eV across the entire Brillouin zone. This is generally favorable for the thermopower as it means that the high Seebeck coefficients generally attained for E_F, the chemical potential, near the band edge will persist to relatively high doping levels if the material can be suitably doped to move E_F closer to the band edge and if a rigid band model is reasonably accurate. We will see that for the four "A" materials, the main effect of such doping is simply to add extra electrons and indeed move E_F closer to the band edge, where the thermoelectric properties are more likely to be optimized.

The high DOS near E_F is also generally favorable for superconductivity, and indeed superconductivity has been observed at 2.1 K (Ref. 22) in the parent compound Mo_3Sb_7.

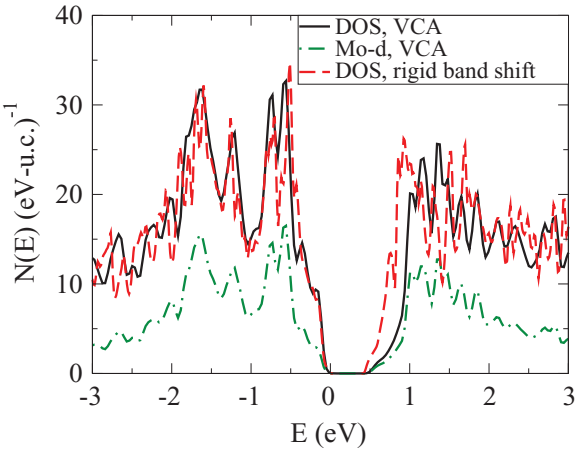

FIG. 3. (Color online) The calculated density of states for the VCA filled-band version of this compound, with the Mo d-character weighting, along with the rigid band shift DOS from Fig. 2(b) shown as well. Note that the band gap of the rigid band DOS has been reduced to facilitate comparison between the VCA and rigid band DOS.

As indicated in the DOS plot, the DOS increases rapidly below E_F, and so it appears that hole doping of this compound, by perhaps niobium or zirconium for the molybdenum, or tin for the antimony, might increase the transition temperature T_c, given the BCS relationship[23] $T_c \propto \exp(-1/\lambda)$ with $\lambda = N(0)V$, where $N(0)$ is the Fermi level DOS and V the interaction strength.

In Fig. 3, we present calculated DOS for the actual parent compound, with zero energy taken not as the Fermi level but as the valence-band edge, along with the VCA calculations described just above (for this calculation, the Fermi level falls naturally at the band edge due to the addition of four electrons per unit cell). The actual calculated band gap in the VCA is somewhat smaller, at 0.53 eV, than the 0.79 eV of the parent compound; to facilitate comparison we have adjusted the band gap for the rigid band case so that the valence and conduction bands of the two calculations are lined up.

A strong similarity between the two DOS plots is immediately apparent, with the basic shape of the valence-band DOS changing very little. The conduction-band DOS shows a somewhat greater disparity, which we speculate may be related to the somewhat different band gap. We have also plotted the weighted molybdenum d state DOS for the stoichiometric compound, which we see to be substantial and, of additional interest, to be of similar shape to the total DOS. This suggests that doping into these same bands, as we are modeling here, is unlikely to produce incoherent scattering, which could hamper conduction.

In Fig. 4, we plot the electronic DOS for each of the four dopants ("$Mo_{2.5}A_{0.5}Sb_7$") as well as for "Mo_2FeSb_7," along with the projected d bands "A"-atom weighting as well as that of Mo. We note first that for all of the plots, the total DOS are very similar, with some changes in the band gap, suggesting the general applicability of a "rigid band" model. In addition, for all of the plots, the Mo d weighting is of the same general shape as the DOS, indicating the basically coherent nature

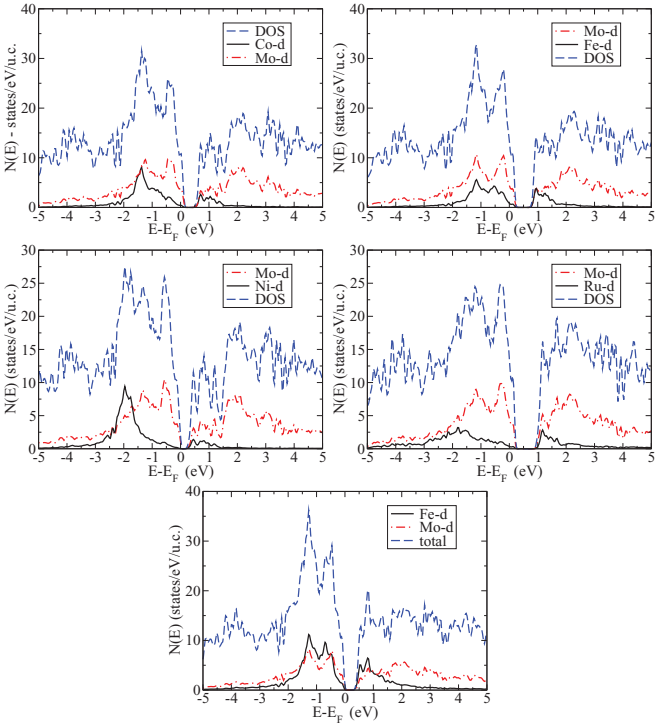

FIG. 4. (Color online) The DFT-calculated densities of states and d character for the hypothetical compounds $Mo_{2.5}Co_{0.5}Sb_7$ (top left), $Mo_{2.5}Fe_{0.5}Sb_7$ (top right), $Mo_{2.5}Ni_{0.5}Sb_7$ (middle left), $Mo_{2.5}Ru_{0.5}Sb_7$ (middle right), and Mo_2FeSb_7 (bottom). Note the generally similar DOS and Mo character plots, as well as the increased Fe weighting in the bottom plot, due to the full atom Fe substitution.

of the transport in the parent compound, consistent with its metallic character.

We turn now to the individual plots, in particular the transition-metal d character. Note that the unit cell contains 6 Mo atoms and 14 Sb atoms, and we are modeling the effect of replacing one ("single substitution") or two Mo atoms ("double substitution") per unit cell. We note that for both the singly substituted $Mo_{2.5}Co_{0.5}Sb_7$ and $Mo_{2.5}Ni_{0.5}Sb_7$ (top left and middle left, respectively), the transition-metal character contains a large peak below the Fermi level—roughly -1.5 eV for Co and -2 eV for Ni—and is of markedly different shape than the Mo character and the overall DOS itself. Although this is largely a qualitative analysis, it suggests that these dopants may increase the electronic scattering and thereby have some impact on transport. In contrast, the singly and doubly substituted Fe plots (top right and bottom, respectively) show Fe d character that is of virtually the same shape as both the DOS and the Mo d character, suggesting that this dopant is likely to be comparatively favorable for transport. This is somewhat surprising given the strongly magnetic nature of Fe, which normally tends to induce strong scattering. One additional advantage of Fe relative to Ni is that it does not appear to reduce the band gap as much as Ni, for example, suggesting a smaller effect on transport. The Ru character plot (middle right) occupies a sort of middle ground, without a strong peak below E_F but not closely following the Mo d character or the DOS.

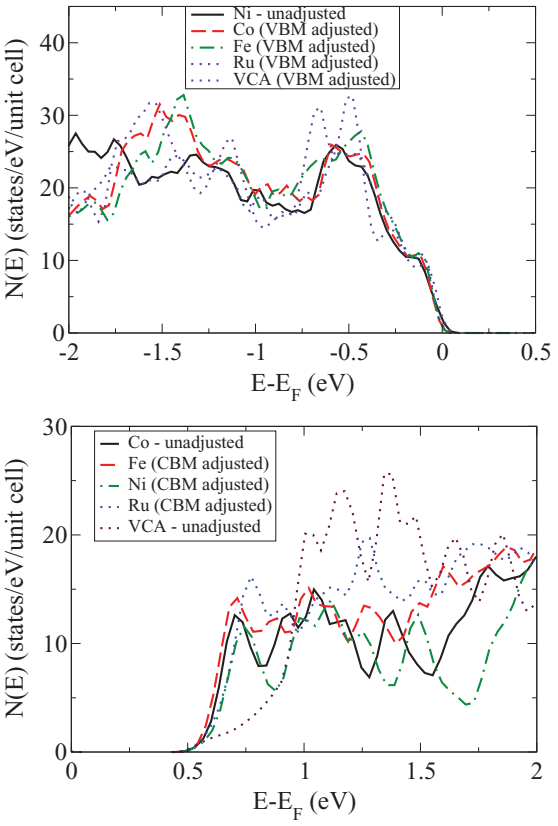

FIG. 5. (Color online) The DFT calculated DOS for each of the indicated singly substituted dopants, for the valence band (Top) and the conduction band (Bottom). Within each figure we have aligned the DOS so that the conduction-band minima and valence-band maxima are aligned, and we have arbitrarily set the conduction-band minimum to be at energy 0.5 eV above E_F; actual calculated band gaps for these four dopants varied between 0.2 and 0.8 eV.

We have focused here on the band character below the gap since to date all samples of doped Mo_3Sb_7 have been found to be *p*-type. However, it is possible that increased efforts at sample preparation may yield *n*-type materials; in general, the same trends as for the subgap character hold true, with the Co and Ru substituted materials perhaps somewhat more favorable for electron doping than for hole doping.

Since the thermopower—a key ingredient of any thermoelectric—is highly sensitive to the shape of the DOS around the band gap, in Figs. 5(a) and 5(b) we have plotted the DOS from the above plots (with the exception of the doubly substituted Fe case) on the same graph. For purposes of comparison, we have aligned the valence- and conduction-band edges for all four dopants, as in Fig. 3. As in the previous figure, the plots are extremely similar for the valence bands; in particular, the rapid rise of the DOS just below the band edge (of prime interest for the thermopower) for the VCA case is well reproduced in each of the four "*A*"-substituted cases. For electron doping, the agreement between the VCA results and the individual substituted compounds is not nearly as good, indicating likely mobility degradation for this case. We focus here on hole doping, where these results generally bode well for doping this material, as comparatively little dopant-to-dopant effects are found. Indeed, the parent compound has been doped with each of these four elements, and while possible solubility limits may come into play here, we think it quite likely that substitutions resulting in a nearly full band will be possible. We have checked the number of electrons that each "*A*" dopant adds to the valence band and find that, as expected from the Periodic Table, each Fe and Ru atom adds two electrons, each Co adds three, and each Ni atom adds four.

In Figs. 6(a) and 6(b), we show the calculated thermopower within the four-electron added VCA for the hole-doped and electron-doped cases, respectively. Although to date samples have only shown *p*-type behavior, it is possible that *n* doping may be achievable, and so we include this as well. The hole thermopower exceeds 350 μV/K near 1000 K for dopings of 0.02 hole/f.u., or roughly 9×10^{19} cm^{-3}, a somewhat heavier doping than that used for Bi_2Te_3. Similar results, if

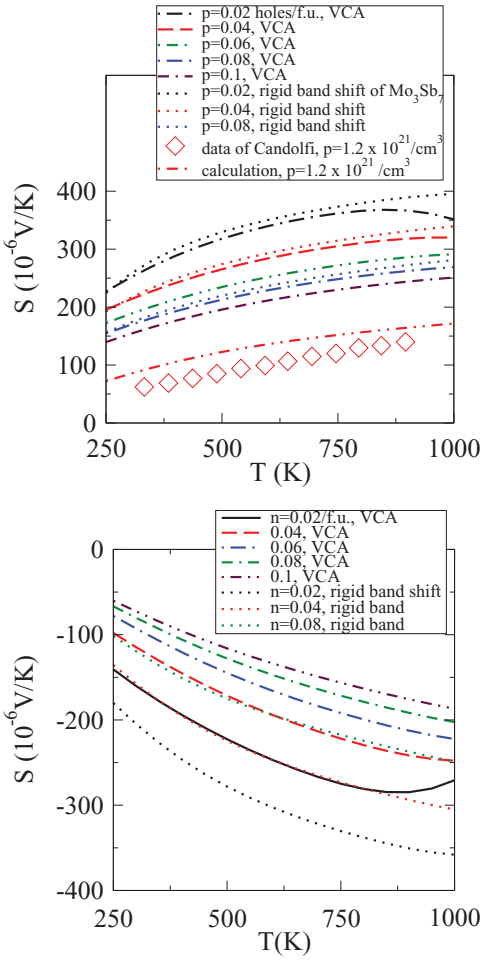

FIG. 6. (Color online) (Top) The hole-doped thermopower S, calculated within the constant relaxation-time approximation using the VCA, is shown at several carrier concentrations, along with (dotted lines) the thermopower within a "rigid band" approach. Note the close similarity between the two below 1000 K, suggesting that the main effect of electron doping is a simple band-filling effect. The disparity at higher temperatures is due to a difference in the band gap, resulting in much larger bipolar conduction effects for the VCA case. We have included a comparison with the data of Candolfi.[7] (Bottom) An analogous plot for electron doping. The disparity between the VCA and rigid band results is due to the different DOS slope near the conduction-band minima (see Fig. 3).

somewhat less impressive, apply on the electron-doped side, with thermopowers at this electron concentration exceeding 250 μV/K near 1000 K. Included in Fig. 6(a) is a direct comparison of our calculation, with *no* adjustable parameters, to the data of Candolfi *et al.*; we see good agreement, indicating the accuracy of our approach. As expected, the achievable thermopower levels are much higher than currently achieved experimentally for doping on the Mo site.

We note that at the lowest doping levels in both plots, the thermopower saturates and begins to "roll over"; this is a direct result of double-sign conduction, wherein the band across the gap begins contributing to the thermopower, but with opposite sign since $\varepsilon - E_F$, where ε is a typical band energy, has switched sign.

With regard to the ultimate performance (i.e., ZT), of course, the conductivity is important and not directly calculated here due to our lack of knowledge of the scattering time τ, which affects the mobility. We can, however, make a "rough and ready" estimate that the "power factor" $S^2\sigma$ may be significantly increased at high temperature, relative to currently achieved levels. To wit, the maximum thermopower in Fig. 6 (achieved for $p = 9 \times 10^{19}$ cm^{-3}) is roughly 2.5 times the corresponding value for $p = 1.2 \times 10^{21}$ cm^{-3}, at approximately 1/13th the carrier concentration. If mobility at these heavy dopings is $\propto p^{-0.6}$, as extracted from experimental data at heavy dopings in our recent study on PbSe,[21] one finds a power factor roughly twice larger at the lower dopings, with a concomitant ZT increase. This is of course a rather rough estimate; without mobility data at these lower concentrations, one cannot make a better estimate.

For completeness, in Figs. 6(a) and 6(b) we have included (dotted lines) computations of the Seebeck coefficient within the "rigid band approximation" for Mo_3Sb_7 doped to a nearly full band. The agreement is excellent below 1000 K for the hole-doped side and somewhat less so for electron doping, generally supporting our assertion that the main effects of doping can be understood within a rigid band model. We note parenthetically that the lack of "rollover" in the rigid band calculations at the highest temperatures is due to the larger band gap, which greatly reduces the effects of double-sign conduction through the thermal factor $df(E - E_F)/dE$ (f is the Fermi function and E is band energy) that typically appears in transport calculations such as the Seebeck coefficient. Since first-principles calculations tend to understate the actual band gap, this suggests that our calculated VCA thermopowers at the highest temperatures may be underestimated; in the absence of hard band-gap data for the substituted compounds, we cannot accurately account for this.

In Figs. 7(a) and 7(b), we show the doping dependence of the thermopower for numerous temperatures between 300 and 1000 K for hole and electron doping, respectively. It is noteworthy that the thermopower is large over a wide temperature range at the dopings of interest, suggesting that if the material is successfully doped, it may show good thermoelectric performance over a wide temperature range. This is of importance for practical applications such as exhaust waste heat recovery, where many elements, each optimized for a different temperature range, must be used.

Although high thermopower is only one of the necessary conditions for a good thermoelectric (the others being low lattice thermal conductivity, high electron mobility, and the ability to sustain large dopings), such large thermopowers at large dopings augur well for the ultimate performance measured as the figure-of-merit ZT.

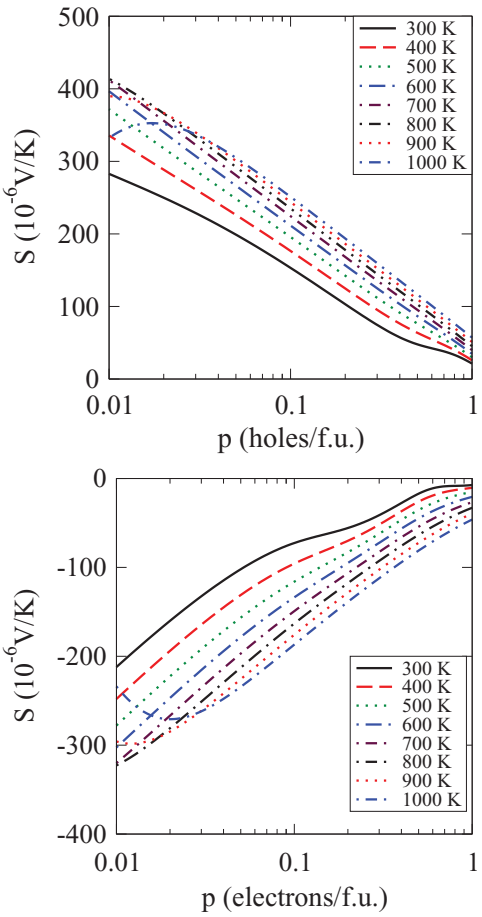

FIG. 7. (Color online) The hole doped (Top) and electron-doped (Bottom) thermopower at various temperatures and dopings, calculated within the VCA as in Fig 5. At dopings above 0.1/f.u., the curves run sequentially by temperature, with lower temperatures having lower absolute thermopowers.

III. LATTICE DYNAMICS

As mentioned previously, we have also performed calculations of the lattice dynamics of the base compound and "A" substituted materials. In Fig. 8, we present calculations of the phonon DOS for the base compound. It displays a separation of the high-energy (above 50 cm^{-1}) spectral weight between the Mo and Sb atoms, with the range between 50 and 175 cm^{-1} almost entirely Sb, and that above mainly Mo; as generally expected, the heavier atom displays lower frequencies, but this effect is much more than would be expected merely based on the mass difference.

Turning to the Ni-substituted phonon DOS in Fig. 9, we see that the nickel, despite only substituting for one of the six Mo atoms, produces a significant amount of spectral weight around 110 cm^{-1}, which is favorable from the standpoint of inducing additional phonon scattering, which may lower the lattice thermal conductivity. As with the Ni-substituted compound,

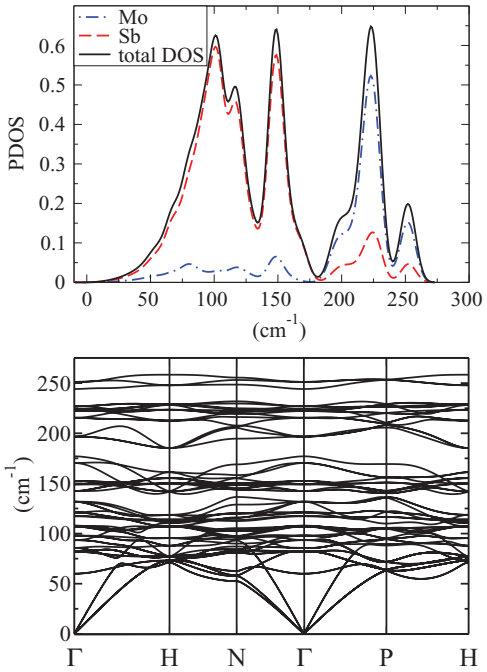

FIG. 8. (Color online) (Top) The phonon density of states for Mo_3S_7. Note that the lower band (between 50 and 175 cm^{-1}) is almost entirely Sb, while the upper band is largely Mo. (Bottom) The phonon band structure for this material. Note the acoustic modes at Γ.

the Co-substituted compound (Fig. 10) shows some lower-energy (relative to the Mo peaks above 200 cm^{-1}) dopant spectral weight, in this case around 150 cm^{-1}, suggesting some enhanced phononic scattering may occur with Co substitution. Of additional interest, there is significant "mixing" of Mo

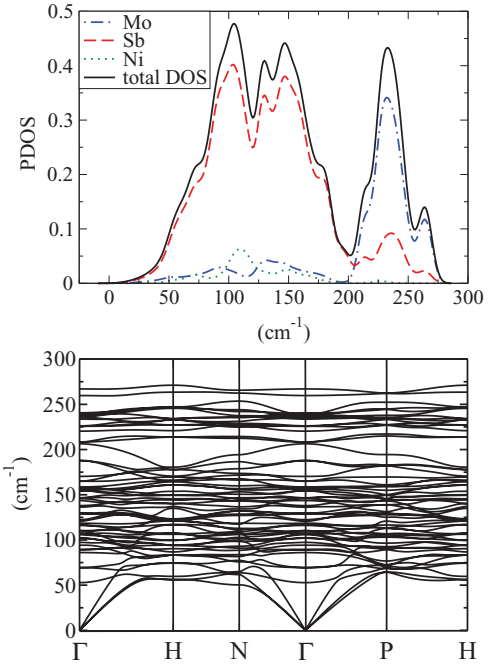

FIG. 9. (Color online) (Top) The phonon density of states for "$Mo_{2.5}Ni_{0.5}Sb_7$." Note the Ni peak around 110 cm^{-1}. (Bottom) The phonon band structure.

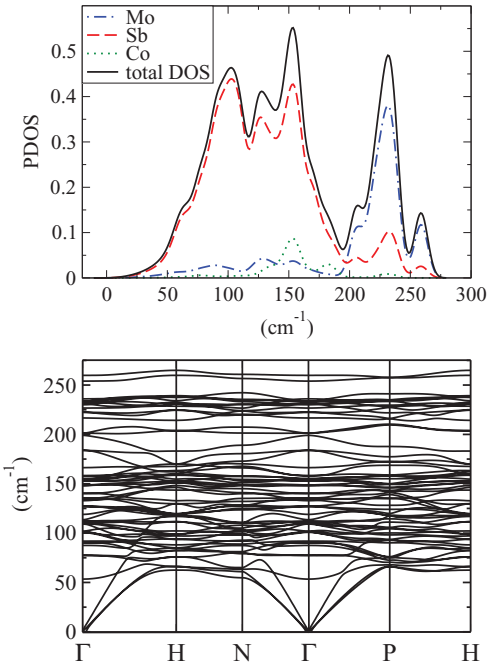

FIG. 10. (Color online) (Top) The phonon density of states for "$Mo_{2.5}Co_{0.5}Sb_7$." Note the Co peak around 150 cm^{-1}. (Bottom) The phonon band structure.

character with the largely Sb character DOS below about 200 cm^{-1}, suggesting that phonon transport in this compound may be less coherent than in the parent compound, again lowering the lattice thermal conductivity. The Fe-doped compound (Fig. 11) shows relatively little low-energy spectral weight of either Mo or Fe, with the Fe peak not present until nearly 200 cm^{-1}, so that, roughly speaking, less phononic scattering may be expected with this dopant. Similar considerations apply to the Ru-doped compound (Fig. 12).

It is worth noting that the phonon spectra differ significantly among themselves, despite the fact that only one atom out of the 20 in the unit cell has been altered and that the elements (Ni, Co, Fe) involved are Periodic Table neighbors. For example, the peaks present in the undoped compound are broader in the Ni-doped compound and much broader in the Co-doped compound. These different behaviors suggest that different phonons may be scattered by different dopants, leading to a beneficial, if modest, reduction in lattice thermal conductivity if dopants are used in combination. As mentioned in the Introduction, if solubility limits come into play, this may be an effective strategy for reducing carrier concentration into an optimal regime. All the materials would generally show Dulong-Petit specific-heat values of approximately 250 J/mol K at the high temperatures studied here.

Included with the phonon DOS plots are phonon band-structure plots for each of the materials studied. These show, in general two nearly degenerate transverse acoustic modes near Γ and a longitudinal mode at somewhat higher frequencies. Given that there are 20 atoms in the unit cell, the plots depict 60 independent phonon bands, with the main apparent difference in the substituted materials being the increased band presence near 175 cm^{-1}, where the pure compound has nearly a gap. In Table I, we present longitudinal and

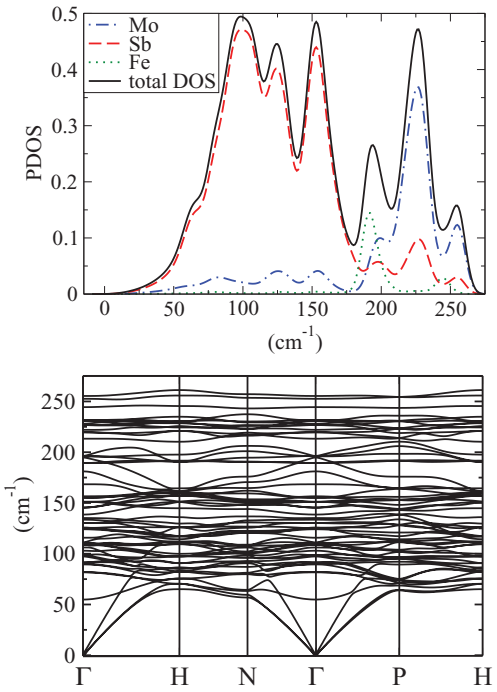

FIG. 11. (Color online) (Top) The phonon density of states for "$Mo_{2.5}Fe_{0.5}Sb_7$." (Bottom) The phonon band structure for this compound.

transverse sound speeds extracted from these plots for each of the five materials studied, in each of the principal crystallographic directions. For the transverse sound speeds, we have averaged over the two polarizations; these two individual speeds generally were within a few percent of each other. The average transverse sound speeds are roughly 10% higher for

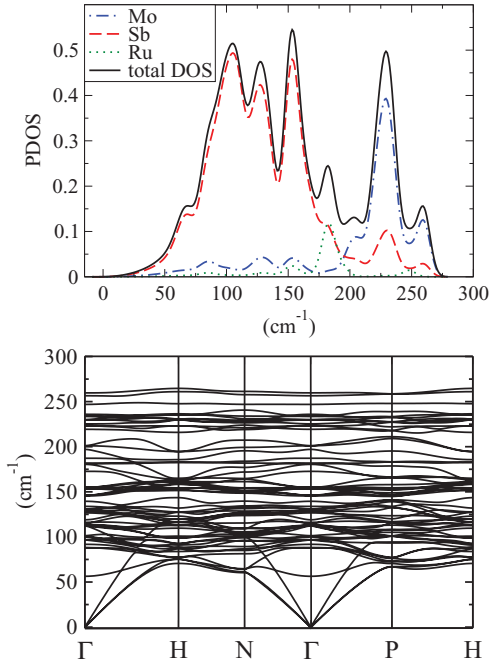

FIG. 12. (Color online) (Top) The phonon density of states for "$Mo_{2.5}Ru_{0.5}Sb_7$." (Bottom) The phonon band structure for this compound.

TABLE I. Sound speeds in m/s extracted from dispersion data.

Compound	Direction	Speed (Trans.)	Speed (Long.)
Mo_3Sb_7	[100]	2750	4810
	[110]	2650	4913
	[111]	2395	4530
Average		**2600**	**4750**
$Mo_{2.5}Ni_{0.5}Sb_7$	[100]	3010	4860
	[110]	2840	4890
	[111]	2780	5040
Average		**2880**	**4930**
$Mo_{2.5}Co_{0.5}Sb_7$	[100]	2890	4830
	[110]	2880	4850
	[111]	2830	4940
Average		**2870**	**4870**
$Mo_{2.5}Fe_{0.5}Sb_7$	[100]	2970	4820
	[110]	2830	4850
	[111]	2850	4910
Average		**2880**	**4860**
$Mo_{2.5}Ru_{0.5}Sb_7$	[100]	2990	4840
	[110]	2860	4980
	[111]	2870	4990
Average		**2910**	**4940**

the substituted cases, while the longitudinal values increase by 2%–4%, so that the mass fluctuation scattering effect in the substituted compounds may be somewhat counteracted by the increased average sound speed. These increases in sound speed are roughly consistent with the decrease in mass from Mo to the transition metals (assuming a constant restoring force). However, the largest sound speed increases are with the Ru substitution, which suggests that the extra electrons added by substitution may well be the relevant quantity affecting sound speeds. This idea—that the extra electrons affect the phonon spectra more than the mass difference—is also borne out by comparing the DOS plots for Fe and Ru (column 8 neighbors in the Periodic Table), which both show dopant spectral weight in the 180–190 cm^{-1} range. The overall spectra for these two dopants are in fact very similar as well.

IV. DISCUSSION AND CONCLUSION

The thermopower and electronic structure calculations of the previous sections suggest that substantially improved thermoelectric performance (relative to that currently achieved) is possible in the heavily substituted Mo_3Sb_7, in particular achievable by transition-metal doping on the molybdenum site. This would lower carrier concentration from that of the presently rather overdoped materials and make the material more semiconductor-like. The electronic structure results suggest that the identity of the dopant is of comparatively little importance, with Fe apparently most favorable from the standpoint of minimizing the resistivity. Our results suggest that each dopant adds the expected number of electrons to the chemically active bands, so that for the thermopower, a simplified "rigid band" model is in fact fairly accurate. Lattice-dynamics calculations indicate some additional phononic scattering due to the dopant addition, suggesting

that the mass fluctuation effect of the substitution may prove effective in reducing the lattice thermal conductivity, but counteracted somewhat by increased sound speeds. We note also that since the material is a superconductor, with concomitantly large electron-phonon interaction, lowering of carrier density via increased doping, as described here, may act to reduce the electron-phonon interaction and thereby increase the mobility.

Regarding the ultimate thermoelectric performance (i.e., ZT), a quantitative estimate is not possible, due to large uncertainty regarding the doping and temperature dependence of the hole mobility at the comparatively lower carrier concentrations (relative to that presently achieved) depicted here. We can say, however, based on the thermopower results, that optimal results are most likely to be found for dopings in the vicinity of 0.02–0.1 holes/f.u., or a carrier concentration of $p = (9 \times 10^{19})$–(4.6×10^{20}) cm^{-3}.

Optimization of this material is, of course, an experimental challenge, and we hope that this work provides additional motivation for further work aimed at doping Mo_3Sb_7 closer to a semiconducting state. We look forward to such efforts with great interest.

ACKNOWLEDGMENTS

Research sponsored by the U.S. Department of Energy, Assistant Secretary for Energy Efficiency and Renewable Energy, Office of Vehicle Technologies, as part of the Propulsion Materials Program, under Contract No. DE-AC05-00OR22725 with UT-Battelle, LLC.

[1] D. Parker and D. J. Singh, J. Appl. Phys. **108**, 083712 (2010).
[2] H. Xu, K. M. Kleinke, T. Holgate, H. Zhang, Z. Su, T. M. Tritt, and H. Kleinke, J. Appl. Phys. **105**, 053703 (2009).
[3] C. Candolfi, B. Lenoir, A. Dauscher, E. Guilmeau, J. Hejtmánek, J. Tobola, B. Wiendlocha, and S. Kaprzyk, Phys. Rev. B **79**, 035114 (2009).
[4] N. Soheilnia, E. Dashjav, and H. Kleinke, Can. J. Chem. **81**, 1157 (2003).
[5] C. Candolfi, B. Lenoir, A. Dauscher, B. Malaman, E. Guilmeau, J. Hejtmanek, and J. Tobola, Appl. Phys. Lett. **96**, 262103 (2010).
[6] C. Candolfi, B. Lenoir, A. Dauscher, J. Hejtmánek, and J. Tobola, Phys. Rev. B **80**, 155127 (2009).
[7] C. Candolfi, B. Lenoir, J. Leszczynski, A. Dauscher, and E. Guilmeau, J. Appl. Phys. **105**, 083701 (2009).
[8] C. Candolfi, B. Lenoir, C. Chubilleau, A. Dauscher, and E. Guilmeau, J. Phys. Condens. Matter **22**, 025801 (2010).
[9] E. Dashjav, A. Szczepenowska, and H. Kleinke, J. Mater. Chem. **12**, 345 (2002).
[10] F. Gascoin, J. Rasmussen, and G. J. Snyder, J. Alloys Compd. **427**, 324 (2007).
[11] H. Zhang, J. He, B. Zhang, Z. Su, T. M. Tritt, N. Soheilnia, and H. Kleinke, J. Electron. Mater. **36**, 727 (2007).
[12] A. F. Ioffe, *Semiconductor Thermoelements and Thermo-electric Cooling* (Inforesearch, London, 1957).
[13] Summary of current production given at [http://minerals.usgs.gov/minerals/pubs/commodity/selenium/mcs-2009-tellu.pdf].
[14] P. Blaha, K. Schwarz, G. K. H. Madsen, D. Kvasnicka, and J. Luitz, *WIEN2k, An Augmented Plane Wave + Local Orbitals Program for Calculating Crystal Properties* (Karlheinz Schwarz, Techn. Universität Wien, Austria, 2001).
[15] G. K. H. Madsen, K. Schwarz, P. Blaha, and D. J. Singh, Phys. Rev. B **68**, 125212 (2003).
[16] A. Togo, F. Oba, and I. Tanaka, Phys. Rev. B **78**, 134106 (2008).
[17] L. Bellaiche and D. Vanderbilt, Phys. Rev. B **61**, 7877 (2000).
[18] A. Kokalj, J. Mol. Graphics Modell. **17**, 176 (1999). Code available from [http://www.xcrysden.org/].
[19] L. Zhang, M.-H. Du, and D. J. Singh, Phys. Rev. B **81**, 075117 (2010).
[20] D. J. Singh, Phys. Rev. B **76**, 085110 (2007).
[21] D. Parker and D. J. Singh, Phys. Rev. B **82**, 035204 (2010).
[22] Z. Bukowski, D. Badurski, J. S. Damm, and R. Troć, Solid State Commun. **123**, 283 (2002).
[23] J. Bardeen, L. N. Cooper, and J. R. Schrieffer, Phys. Rev. **108**, 1175 (1957).